Water slip and friction at a solid surface

2008 J. Phys.: Condens. Matter 20 354016

(http://iopscience.iop.org/0953-8984/20/35/354016)

J. Phys.: Condens. Matter **20** (2008) 354016 (5pp) doi:10.1088/0953-8984/20/35/354016

Water slip and friction at a solid surface

L Brigo[1,2], M Natali[3], M Pierno[1,2], F Mammano[1,4], C Sada[1,2], G Fois[1,2], A Pozzato[1,5], S dal Zilio[1,5], M Tormen[5] and G Mistura[1,2,6]

[1] Dipartimento di Fisica G Galilei, Università degli Studi di Padova, via Marzolo 8, 35131 Padova, Italy
[2] Consorzio Nazionale Interuniversitario per le Scienze Fisiche della Materia (CNISM), Via della Vasca Navale 84, 00146 Roma, Italy
[3] Istituto di Chimica Inorganica e delle Superfici (ICIS), CNR, Corso Stati Uniti 4, 35127 Padova, Italy
[4] Venetian Institute of Molecular Medicine (VIMM), Via Orus 2, 35129 Padova, Italy
[5] TASC-INFM, CNR, S S 14 km 163.5 Area Science Park, 34012 Basovizza, Trieste, Italy

E-mail: mistura@padova.infm.it

Received 1 February 2008, in final form 3 March 2008
Published 11 August 2008
Online at stacks.iop.org/JPhysCM/20/354016

Abstract
A versatile micro-particle imaging velocimetry (μ-PIV) recording system is described, which allows us to make fluid velocity measurements in a wide range of flow conditions both inside microchannels and at liquid–solid interfaces by using epifluorescence and total internal reflection fluorescence excitation. This set-up has been applied to study the slippage of water over flat surfaces characterized by different degrees of hydrophobicity and the effects that a grooved surface has on the fluid flow inside a microchannel. Preliminary measurements of the slip length of water past various flat surfaces show no significant dependence on the contact angle.

1. Introduction

Microfluidics is an emerging, highly interdisciplinary field of science and technology, lying at the interface between physics, chemistry, engineering and molecular biology [1]. Microfluidics currently attracts great industrial and academic interest due to its numerous potential applications and its scientific fascination [2].

A common feature to all microfluidic chips is their large surface-to-volume ratio. Accordingly, the behavior of such devices is dominated by the interfacial properties. Examples include spatial confinement of liquid streams by modulation of wetting properties [3] and driving of liquid flows by capillarity [4] and by electro-osmosis [5].

A topic which has recently drawn a lot of attention [6–8] concerns the validity of the 'no-slip' boundary condition, because of its fundamental relevance for the dynamics at the solid–fluid interface and because of the important role that drag reduction could play in microfluidic channels. The slip length is the distance behind the interface at which the liquid velocity extrapolates to zero. On nominally flat hydrophobic surfaces, it generally is rather small and lies in the range 10 nm–1 μm, which explains why the 'no-slip' boundary condition is considered a good approximation in macroscopic flows. Nevertheless, in several micro/nanofluidic devices, the effect of a finite slip length on the fluid dynamics becomes important in channels of micrometer or nanometer size.

Many techniques [7] have been successfully applied to investigate the liquid flow over a solid surface, which either measure forces between moving objects, like the atomic force microscope (AFM) [9] and the surface force apparatus [10], or image the flows using tracing molecules or particles, like fluorescent spectroscopy after photobleaching [11] and double focus fluorescence cross-correlation [12]. Particle imaging velocimetry (PIV) is a well established technique for measuring fluid velocities in macroscopic flows. Typically, the positions of tracing particles are followed and their velocity determined by cross-correlating images obtained at small time intervals. Recently, its spatial resolution has been improved in order to investigate flow patterns inside microchannels and close to liquid–solid interfaces [13, 14].

Hereafter, we report the development of a μ-PIV set-up that is sufficiently versatile to image a wide range of flow conditions encountered in microfluidic devices, allowing the determination of fluid flow velocities both in the bulk of the fluid by epifluorescence microscopy and at the interface with a transparent solid surface by the use of total-internal-

[6] Author to whom any correspondence should be addressed.

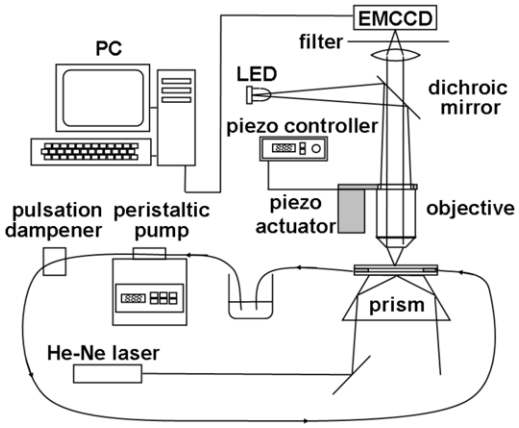

Figure 1. Schematic diagram of the optical measurement system set-up.

reflection (TIR) fluorescence microscopy. This latter feature is quite important for the study of slippage phenomena and it represents an upgrade with respect to previous set-ups [13, 14]. We have applied it to study the slippage of water over flat surfaces having different degrees of hydrophobicity and the effects that a grooved surface has on the flow of a fluid moving in a microchannel.

2. Experimental set-up

Figure 1 shows a scheme of the imaging system that we have designed and assembled, and that we are currently employing as a μ-PIV recording system.

A microfluidic flow cell is realized either through a commercial close bath chamber (RC-30, Warner Instruments), housing a silicone gasket sandwiched between top and bottom glass cover-slips (respectively 0.15 and 1 mm thick), held in place by mechanical pressure, or through flow chambers made of glass and thiolene-based optical adhesives (NOA, Norland Products) fabricated by using rapid prototyping soft-lithographic techniques [15]. Both types of fluidic cell are provided with channels a few hundred micrometers deep and a few millimeters wide for the perfusate to traverse.

The microfluidic flow cell is mounted on a microscope that allows two different configurations for sample illumination: (1) epiluminescence (light from above the sample) and (2) total internal reflection (TIR), with the sample illuminated from below.

In the first mode, light is introduced through a horizontal aperture of a vertical tube which houses various components of the microscope. As an illumination source we have chosen a red helium–neon laser (model 05-LHR-211, Melles Griot, 5 mW maximum output power at 632.8 nm) because of its wide availability and low cost. In order to allow future economic solutions for changing excitation wavelength, we have also tested high brightness LEDs for epifluorescence illumination. For instance, we have realized a battery of seven super-bright LEDs (Precision Optical Performance AlInGaP LEDs, Agilent Technologies), characterized by 635 nm peak wavelength, 17 nm spectral half-width, 9300–16 000 mcd luminous intensity at 20 mA and 6° viewing angle. In the case of epiluminescence, despite a lower contrast imaging, no significant difference was observed between the LED array and the He–Ne laser.

A dichroic mirror (model z633rdc, Chroma, USA) reflects the light of the source used to illuminate the sample from above and transmits the emission spectrum to the camera (nominal transmitted light: 5% at $\lambda = 633$ nm, 9% at $\lambda = 635$ nm, and 63% at $\lambda = 645$ nm). A filter (model HQ 675/50 m, Chroma, USA) is placed in front of the camera, in order to cut off the excitation scattered light.

The incoming light excites the fluorescence of specific tracing particles dispersed in water. The measurements presented in this work were acquired with 1 μm diameter polystyrene spheres loaded with fluorescent dyes which absorb at $\lambda_{abs} = 625$ nm and emit at $\lambda_{em} = 645$ nm (molecular probes, Invitrogen).

The emitted fluorescent light is collected by the objective lens. We used a 63× magnification, water immersion objective with a numerical aperture (NA) of 0.9 (HCX APO L U-V-I, Leica), whose vertical position can be fine adjusted with a piezoelectric nanopositioning system (MIPOS 250, Piezosystem Jena) with 5 nm resolution and 60 nm repeatability.

The TIR illumination configuration is obtained by placing a trapezoidal prism made of flint glass (refraction index $n_f = 1.599$ at $\lambda = 633$ nm) below the sample. The system is aligned so that TIR takes place in the flow cell at the interface between the microchannel floor and the working fluid. In order to reduce laser light escape due to reflections, the flow cell bottom cover-slip is put in optical contact with the prism upper base surface by a layer of immersion oil, while the flow cell top cover-slip is put in optical contact with the objective by ophthalmic gel. The beam, directed upwards, traverses the prism lower base normally, is reflected at the 60° inclined lateral surface and reaches the upper base under an angle of 60°, which is sufficiently high to satisfy the TIR condition on the surface of the sample. Accordingly, the evanescent field extends inside the microchannel from the glass base surface upwards for about 130 nm, with exponentially decreasing intensity. The prism is made out of flint glass because of its high refraction index value (higher than the $n = 1.52$ of ordinary optics glass), making the realization of the geometric conditions to obtain TIR easier, and because of its low native luminescence at the working wavelengths. We have found that the light intensity from a 5 mW maximum power He–Ne laser is sufficient to get useful TIR images. We have also tried using LED illumination in TIR configuration but with no success: in fact, the relatively large LED light beam divergence makes the alignment procedure necessary to realize the TIR condition definitely difficult. As a consequence, the evanescent field is masked by the unavoidable presence of spurious transmitted light.

Finally, the detector is a recently commercialized electron multiplying charge coupled device EMCCD detector with a 658×496 pixel array (corresponding to a 6.58×4.96 mm^2 real image), 14 bit resolution and real time electron multiplier gain control (Luca, Andor Technology). The camera is cooled down

to −20 °C to lower the readout noise from the CCD detector. Moreover, binning allows charge from two or more pixels to be combined on the EMCCD chip prior to readout, giving even better noise performance at the expense of spatial resolution. Using the 63× microscope objective described above, the field of view is 104 × 79 μm^2.

The flow chamber is filled by a solution of fluorescent beads that is prepared by diluting the commercial product in deionized water so that a suitable quantity of liquid and density of beads in the μ-PIV images is obtained (80 μl commercial bead solution in a few milliliters of deionized water), taking care that no air bubbles are trapped inside the perfusion cell during its initial filling. A peristaltic pump (Minipuls 3 equipped with standard pump head, Gilson) is connected to the chamber through a homemade microfluidic dampener of pressure pulsations in order to produce a uniform flow.

3. Flow past flat surfaces

As a first application of this μ-PIV set-up, we studied water slippage in wide microfluidic channels (width 3 mm, length 4 cm) formed by a silicone gasket sandwiched between top and bottom glass cover-slips (respectively 0.15 mm and 1 mm thick). The nominal height of the channels was 100 μm, although the actual depth could be doubled because of the use of vacuum grease to seal the flow chamber. Vacuum grease does not contaminate the channel floor and ceiling, while the fluid–grease contact area on the lateral surfaces is kept as small as possible. The bottom glass surface was coated with different substances characterized by very diverse contact angles. In particular, thin layers of polydimethylsiloxane (PDMS) and of a thiolenic glue (NOA) were spin coated on bare glass slides and successively exposed to UV light for curing. We chose these two polymers because they are commonly used in rapid prototyping of microfluidic chips [15]. The glass surface was also functionalized with a self-assembled monolayer of octadecyltrichlorosilane (OTS) and of perfluorooctyltrichlorosilane (TPOS). The roughness of the bare and coated glass slides was determined with an AFM. Typical roughness values of a few nanometers over scan areas of 30 μm × 30 μm were found. No significant difference was observed between the bare and the coated glass surface. A microfluidic cell that presents a channel 250 μm deep and 6.5 mm wide with lateral and bottom walls in NOA and a top wall in glass was also fabricated by soft-photolithographic techniques [15].

The measurement of water contact angles Θ on the various channel bottoms yielded the following values: bare glass $\Theta = (22 \pm 3)°$, NOA $\Theta = (77 \pm 3)°$, TPOS $\Theta = (103 \pm 2)°$, OTS $\Theta = (108 \pm 2)°$ and PDMS $\Theta = (120 \pm 1)°$, which are consistent with standard values.

Figure 2 shows the velocity profile measured in a channel presenting a flat NOA floor and a glass ceiling for a flow rate $Q \approx 80$ nl s^{-1}. The position of the bottom channel wall was roughly determined using white light from a mercury lamp and focusing the beads that are stuck to the bottom glass slide. For a more accurate determination, the He–Ne laser was switched on and the objective position was fine regulated through the piezoelectric actuator in order to image those tracers whose fluorescence is excited by the evanescent field, which extends from the microchannel floor up in the liquid to a ∼130 nm height. We associated with such a determination a (systematic) uncertainty of ∼100 nm.

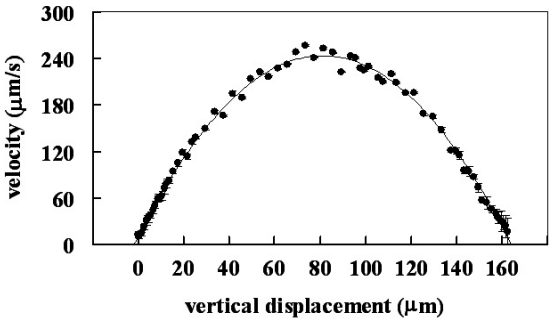

Figure 2. Velocity profile measured in a 162 μm deep channel presenting a flat NOA floor and glass ceiling for $Q \approx 79$ nl s^{-1}.

Double exposure images and/or sequences of single exposure images were recorded. We set exposure times and time intervals between exposures so as to acquire 'meaningful' μ-PIV images from the middle of the channel, where the highest fluid velocity is expected. For example, for the profile shown in figure 2, the CCD array was exposed for $\Delta t_{\text{exp}} = 2$ ms and a series of eight successive single exposure images was acquired with a time delay $\Delta t_{\text{del}} = 70$ ms (∼14 Hz). Each experimental point in the plot represents the modulus of the average value of the velocity field, returned by the EDPIV [16] ensemble correlation analysis, relative to each vertical position inside the channel. The direction of the velocity vectors in each velocity field can be considered constant within low errors (<1°), as expected in a microfluidic laminar flow. The statistical error affecting the velocity measurements is lower than the point dimensions in the plot. By varying the voltage applied to the piezoelectric nanopositioning device, μ-PIV images can be recorded for different positions of the focus within the channel, spanning from the bottom wall up to a 200 μm distance, that is the maximum elongation of the piezoelectric stage.

The slip length b was deduced by applying least squares parabolic fits to the data: b is the difference between the measured position of the wall z_{wall} and the extrapolation of this parabola to zero. In practice, we extrapolated several values for b, using different groups of experimental points which are separated from the surface by distances larger than about one bead diameter [14] to avoid electrostatic repulsion effects between the particles and the wall [12]. The slip length is then the average of the values derived by the various fits.

The results for the different flat surfaces are $b_{\text{glass}} = 0.10 \pm 0.09$ μm, $b_{\text{NOA}} = 0.8 \pm 0.3$ μm, $b_{\text{TPOS}} = 0.8 \pm 0.3$ μm, $b_{\text{OTS}} = 0.5 \pm 0.2$ μm and $b_{\text{PDMS}} = 0.9 \pm 0.8$ μm and refer to typical shear rates at the wall less than about 10 s^{-1}. The statistical error represents one standard deviation of the values, to which one must add the systematic uncertainty in the determination of the actual position of the wall from TIR images, equal to about ± 0.10 μm. Apart from the large error bars, probably related to the use of big tracers and of

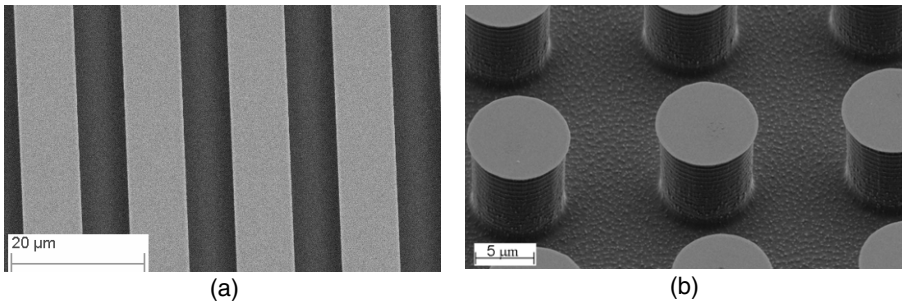

Figure 3. SEM images of silicon masters patterned with canals 8 μm wide, 3 μm deep and of 15 μm period (a) and with pillars 8 μm wide, 3 μm high, located on a square grid of period 16 μm (b).

an objective with a small NA, our results do not show any systematic dependence of b on the contact angle of the surface. They are also consistent with those obtained by Joseph and Tabeling from PIV measurements at much larger shear rates at the wall [14]. In the case of OTS, our result is intermediate between that observed by Joseph and Tabeling [14], $b = 57 \pm 100$ nm, and that measured by Tretheway and Meinhart [13], $b = 1 \pm 0.45$ μm.

4. Flow past microstructured surfaces

We have also investigated the flow near a microstructured wall. Glass slides coated with a patterned NOA layer were prepared, see figure 3, starting from silicon masters produced with standard photolithography and wet etching techniques. The negative in PDMS of the silicon master, realized by replica molding, served as a mold for the replica of the positive pattern in NOA, which was glued on a thin glass slide for mechanical stability. In this way, patterns consisting of a series of cylindrical pillars and dots and of rectangular wells were produced. Each patterned slide was then mounted in the flow chamber, to serve as a microchannel floor.

The plot of figure 4 shows the velocity profile measured in the proximity of an NOA floor presenting a regular pattern of pillars (diameter 8 μm, height 3 μm located on a square grid of period $\Lambda = 16$ μm) and a bare glass ceiling. The height H of the channel was estimated to be 300 μm, therefore we are in the regime of distant plates $H \gg \Lambda$, where the perturbation due to the pillars is expected to produce effects localized to the vicinity of the surface [17]. The wall position was experimentally determined using TIRF and white light imaging. The origin of the z axis to is assumed to be the plane supporting the pillars.

Estimates of the slip length were deduced by applying least squares linear fits to the data points: b is then the opposite of the intercept of the fitting line. Again, to avoid artefacts at the interface, variable data windows were considered in the analysis, starting from a distance of about one bead diameter from the surface (see the gray box in figure 4). The slip length is the average of the values given by the different fits. For the array of pillars in NOA we found $b_{\text{pill}} = -2.10 \pm 0.50$ (stat) ± 0.10 (syst) μm. A negative slip length means that the flat bottom no-slip surface is located at a height b_{pill} from the wall, i.e. in the liquid phase. As expected, the presence

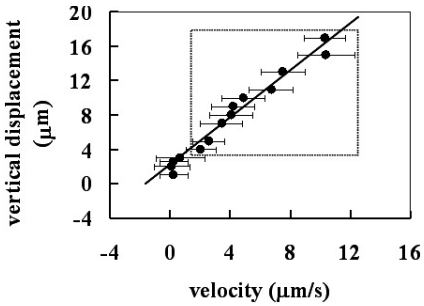

Figure 4. Velocity profile measured near a pattern of pillars in NOA. The box shows a window of data selected for a linear fit to determine an estimate of b.

of the microscopic pillars increases the overall hydrodynamic resistance of the surface [17].

Using the above mentioned techniques, we also fabricated glass slides coated with an NOA layer that presents a pattern of linear grooves. The linear grooves are variably oriented with respect to the channel axis, which corresponds to the applied pressure gradient direction. Here we present the data obtained with an array of grooves 8 μm wide, 3 μm high and with a period $\Lambda = 15$ μm patterned on the bottom surface of a rectangular channel having a height $H = 300$ μm. The position of the groove bottom and top can be experimentally determined using both TIRF and white light imaging. Actually, the presence of a patterned interface determines laser light scattering in the liquid: a clean laser TIR signal was found only when the channels were oriented parallel to the plane defined by the laser path inside the prism. In the other cases, white light imaging helped establish the interface location. Thus, the origin of the z axis was located at half pattern amplitude. Furthermore, by means of white illumination, it was possible to detect the orientation of the grooves and refer it to the pressure gradient direction as defined by the μ-PIV vector field measured far from the microchannel walls (see figure 5).

It is known that a closed channel with a grooved floor, with the grooves forming an angle with the axis of the channel, induces a helicoidal pattern of the streamlines [17], which can be exploited to favor mixing streams of steady pressure-driven flows in microchannels at low Reynolds numbers [18]. We studied the transverse motion induced in the flow by a bottom floor which presented in its central section over a distance of about 1 cm a pattern 8–15 variably oriented with respect to the

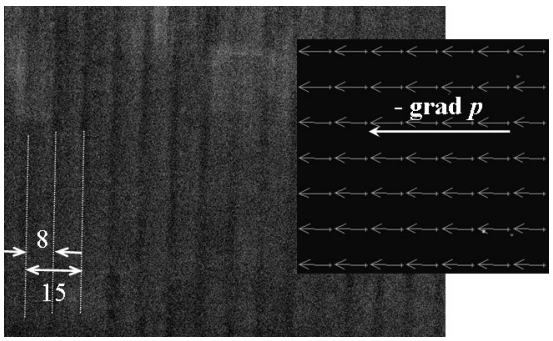

Figure 5. White light recording of the microchannel bottom consisting of an array of parallel grooves (left) perpendicularly oriented with respect to the pressure gradient direction defined by the flow field measured far from the microchannel walls (right).

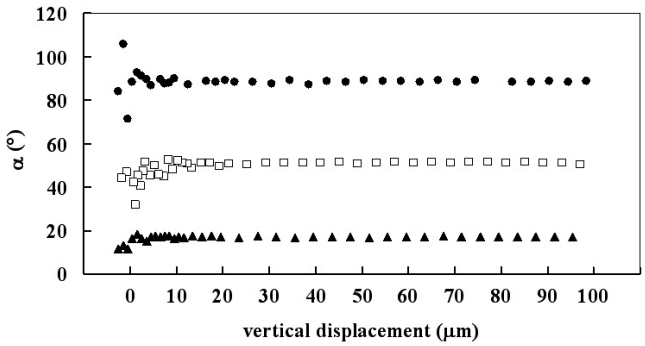

Figure 6. Angle α between the direction defined by the μ-PIV vector field and the direction of the grooves on the floor of the microchannel as a function of the distance from the interface for grooves oriented (●) perpendicularly, (▲) almost parallel and (□) obliquely with respect to the pressure gradient direction.

channel axis. The channel length, $L = 4$ cm, much larger than the overall size of the patterned region, about 2 cm, guarantees that in the middle of the grooved section the flow is not affected by entrance effects.

Figure 6 shows the angle between the direction defined by the μ-PIV vector field at a certain distance from the interface and the direction of the linear grooves, for three different orientations of the pattern: almost parallel to the channel direction with which it forms an angle $\alpha = 17°$, oblique ($\alpha = 52°$) and perpendicular ($\alpha = 89°$).

We see that after a few microns from the groove top, corresponding to a distance equivalent to a couple of times the groove height, the flow field follows the direction of the pressure gradient. For smaller distances, the flow is affected by the underlying pattern and a small deviation towards the groove direction is observed. Interestingly, close to the perpendicular pattern, tracers are found to deviate from the channel axis, and due to the symmetry of the system they are equally found deviating to the right and to left. More measurements are in progress to better quantify these effects.

5. Conclusions

We have realized a low cost micro-particle imaging velocimetry recording system which combines standard epifluorescence illumination with total internal reflection excitation. To show its versatility, we have studied the slippage of water over flat surfaces having different degrees of hydrophobicity and the effects that a grooved surface has on the flow of a fluid moving in a microchannel. Preliminary measurements of the slip length carried out with fluorescent tracers having a diameter of 1 μm are consistent with those obtained by Joseph and Tabeling from PIV measurements at much larger shear rates at the wall [14]. More systematic measurements are planned with an upgraded set-up, comprising an objective of larger NA, and the use of smaller tracing particles. These will be extended to liquids more viscous than pure water in order to verify the influence of the surface treatments.

Acknowledgments

We wish to thank Paolo Parisotto for his expert technical assistance and also Stefano Begolo and Ciro Semprebon for their kind help. Partial support from MIUR-PRIN contract 2006023721 and from CNISM-CNR Progetto d'Innesco della Ricerca Esplorativa 2007 'Viscous flows in microfluidic devices' are warmly acknowledged.

References

[1] Tabeling P 2006 *Introduction to Microfluidics* (New York: Oxford University Press)
[2] Squires T M and Quake S R 2005 *Rev. Mod. Phys.* **77** 977
[3] Zhao B, Moore J S and Beebe D J 2001 *Science* **291** 1023
[4] Lam P, Wynne K J and Wnek G E 2002 *Langmuir* **18** 948
[5] Ajdari A 1996 *Phys. Rev.* E **53** 4996
[6] Granick S, Zhu Y and Lee H 2003 *Nat. Mater.* **2** 221
[7] Neto C, Evans D R, Bonaccurso E, Butt H J and Craig V S J 2005 *Rep. Prog. Phys.* **68** 2859
[8] Bocquet L and Barrat J L 2007 *Soft Matter* **3** 685
[9] Craig V S J, Neto C and Williams D R M 2001 *Phys. Rev. Lett.* **87** 054504
[10] Zhu Y and Granick S 2002 *Phys. Rev. Lett.* **88** 106102
[11] Pit R, Hervet H and Léger L 2000 *Phys. Rev. Lett.* **85** 980
[12] Lumma D, Best A, Gansen A, Feuillebois F, Rädler J O and Vinogradova O I 2003 *Phys. Rev.* E **67** 056313
[13] Tretheway D C and Meinhart C D 2002 *Phys. Fluids* **14** L9
[14] Joseph P and Tabeling P 2005 *Phys. Rev.* E **71** 035303
[15] Natali M, Begolo S, Carofiglio T and Mistura G 2008 *Lab Chip* **8** 492
[16] EDPIV is available at http://eo.yifan.net/users/l/lcgui/Edpiv_intro.htm
[17] Stroock A D, Dertinger S K, Whitesides G M and Ajdari A 2002 *Anal. Chem.* **74** 5306–12
[18] Stroock A D, Dertinger S K, Ajdari A, Mezic I, Stone H A and Whitesides G M 2002 *Science* **295** 647